

This work was written as part of one of the author's official duties as an Employee of the United States Government and is therefore a work of the United States Government. In accordance with 17 U.S.C. 105, no copyright protection is available for such works under U.S. Law.

Public Domain Mark 1.0

<https://creativecommons.org/publicdomain/mark/1.0/>

Access to this work was provided by the University of Maryland, Baltimore County (UMBC) ScholarWorks@UMBC digital repository on the Maryland Shared Open Access (MD-SOAR) platform.

**Please provide feedback**

Please support the ScholarWorks@UMBC repository by emailing [scholarworks-group@umbc.edu](mailto:scholarworks-group@umbc.edu) and telling us what having access to this work means to you and why it's important to you. Thank you.



# Cloud remote sensing with EPIC/DSCOVR observations: A sensitivity study with radiative transfer simulations

Meng Gao<sup>a</sup>, Peng-Wang Zhai<sup>b,\*</sup>, Yuekui Yang<sup>c</sup>, Yongxiang Hu<sup>d</sup>

<sup>a</sup>SSAI/NASA Goddard Space Flight Center, Ocean Ecology Laboratory, Greenbelt, MD, USA

<sup>b</sup>JCET/Department of Physics, University of Maryland Baltimore County, Baltimore, MD, 21250, USA

<sup>c</sup>NASA Goddard Space Flight Center, Climate and Radiation Laboratory, Greenbelt, MD, USA

<sup>d</sup>MS 475 NASA Langley Research Center, Hampton, VA 23681-2199

## ARTICLE INFO

### Article history:

Received 14 December 2018

Revised 28 March 2019

Accepted 28 March 2019

Available online 29 March 2019

### PACS:

42.68.-w

42.68.Ay

42.68.Mj

### Keywords:

Atmospheric and ocean optics

Propagation, transmission, attenuation, and radiative transfer

Scattering

Polarization

## ABSTRACT

The Earth Polychromatic Imaging Camera (EPIC) onboard the Deep Space Climate Observatory (DSCOVR) views nearly the whole sunlit face of the Earth with 10 spectral bands ranging from the UV to the near-infrared, including two oxygen absorbing bands centered at 764 nm (A-band) and 687.75 nm (B-band). Clouds are among the primary remote sensing targets using EPIC images because of their important impacts on the Earth's radiation budget. In order to facilitate the EPIC cloud data product development, we have built a radiative transfer simulator featuring flexible cloud microphysical parameters, gas absorptions, and the instrument line shape functions for each EPIC band. The radiative transfer simulator is used to explore the sensitivity of EPIC observations on liquid-phase cloud microphysical parameters, including optical depth, geometric thickness, and cloud top height. We found that the ratios of the reflectances in the oxygen A and B bands to their respective continuum measurements can be used to increase the confidence level of cloud masking over scenes with sun-glint. In addition, the 388 nm band can be used to differentiate low and high clouds with the uncertainty of roughly 2–3 km. Combining this information with the oxygen absorption bands, the cloud geometric thickness can be obtained with the rough uncertainty of 3–4 km.

© 2019 Elsevier Ltd. All rights reserved.

## 1. Introduction

The Earth Polychromatic Imaging Camera (EPIC) onboard the Deep Space Climate Observatory (DSCOVR) acquires at least 9–12 images of the sunlit side of the Earth daily from the first Lagrange point (L1) of the Sun-Earth orbit, which is approximately 1.5 million km from the Earth [1]. The EPIC bands cover wavelengths from UV (317.5 nm, 325 nm, 340 nm, and 388 nm), visible (443 nm, 551 nm, 680 nm, and 687.75 nm) and near infrared (764.0 nm, and 780 nm), which have important science applications in the remote sensing of the total column ozone, aerosol index, and UV reflectance at the Earth's surface [2]; SO<sub>2</sub> [1], clouds [3–6], vegetation [7], and detection of horizontally oriented ice plates [7].

Cloud masking is among the highest priorities of the numerous applications of the EPIC images including atmospheric correction [8], aerosol remote sensing [9], ocean color [10], just to list a few. Cloud masking over sun glint is a challenging task as sun glint is very bright and a thin cloud layer above it may reduce or

increase the reflectance at the top of the atmosphere (TOA) depending on the viewing geometry. This makes simple reflectance threshold methods unreliable [11,12]. Improvements of cloud masking have been made by using infrared bands [13], which unfortunately are not available in EPIC bands. A reliable cloud mask algorithm over sun glint is especially important for EPIC data processing because it occupies a significant portion of each image.

Cloud optical depth (COD), cloud top height (CTH), and cloud geometric thickness (CGT) are among the primary remote sensing parameters, which are critical to climate modeling [14]. It is relatively straight forward to retrieve COD from EPIC visible bands [7]. Yang et al. [3] explored the possibility of retrieving both CTH and CGT using the different photon path length distribution in the oxygen A and B bands. Davis et al. [4,5] later demonstrated that only one variable in CTH and CGT can be retrieved from the EPIC oxygen A and B bands after considering the instrument noise. Radiative transfer theory suggests that the strong wavelength dependence of Rayleigh scattering can be used to retrieve CTH [15]. In this sense, the UV bands are most sensitive to CTH as larger CTH decreases the amount of molecular scattering, which are prominent in this

\* Corresponding author.

E-mail address: [pwzhai@umbc.edu](mailto:pwzhai@umbc.edu) (P.-W. Zhai).

wavelength range. The possibility of retrieving CTH with the EPIC UV bands is not explored yet in the literature.

In order to facilitate the algorithm development for cloud remote sensing, we have developed a radiative transfer simulator for the EPIC measurements. The details of the simulator is described below in Section 2. The simulator can be used to perform sensitivity study of retrieving different parameters from the EPIC images. In particular, we have used this simulator to study the possibility of retrieving CTH using the EPIC 388 nm band, which in turn can be used as an input to the oxygen A and B band lookup tables for retrieving CGT [3]. Moreover, we have studied the possibility of performing cloud masking over sun glint using  $R_{abs}/R_{ref}$ , where  $R$  stands for reflectance measured by EPIC, and the subscript *abs* refers to the oxygen A (centered at 764 nm) or B (centered at 687.75 nm) bands, and *ref* represents the continuum band centered at 780 nm or 680 nm paired with the oxygen A or B bands, respectively. Both sensitivity studies are important for improving the cloud data products for EPIC observations [6] and have not been done before.

This paper is organized as follows. Section 2 describes the radiative transfer simulator for EPIC. In Section 3 the simulator is used to calculate the ratio of  $R_{764}/R_{780}$  for a hypothetical hydrosphere (no land surface) to explore the possibility of cloud masking using the oxygen A band. Section 4 shows the sensitivity of the EPIC measurement at 388 nm to the CTH variation. We summarize the results in Section 5.

## 2. Radiative transfer simulator for EPIC

The EPIC simulator is built upon a radiative transfer model, which is based on the successive order of scattering (SOS) method [16–19]. The radiative transfer model solves multiple scattering of monochromatic light in the atmosphere and surface system. The formulas of the SOS method is physics based which provide more insights on how each order of scattering contributes to the total radiance field [20]. After years of development, our model has been well validated against the matrix operator method [21], Monte Carlo method [22], and Markov chain method [23]. Gas absorptions due to ozone, oxygen, water vapor, nitrogen dioxide, methane, and carbon dioxide have been incorporated in all EPIC bands. For water vapor, oxygen, carbon dioxide, and methane, we used the atmospheric radiative transfer simulator (ARTS) [24] and the HITRAN2012 database [25] to build a hyperspectral lookup table of the gas absorption coefficients. Absorptions by ozone and nitrogen dioxide are included by interpolating the measurements in [26,27], respectively. In the oxygen A and B bands, we performed line-by-line simulations inside the measurement bands and then convoluted the radiance at the top of the atmosphere with the EPIC instrument line shape function. For other bands, we first calculated the average absorption coefficients within the instrument line shape function, then coupled the average absorption coefficients with the multiple scattering solution in the radiative transfer model to simulate the EPIC detector response.

The atmosphere is assumed to be a three-layer medium. The top layer is a molecule layer, which scatters according to the Rayleigh scattering matrix with the depolarization of 0.0284 [28]. The middle layer is a mixture of scattering particles and molecules. The scattering particles can be aerosols or cloud particles. In this work we have assumed the scattering particles as water cloud droplets, which follow the gamma size distribution, with the effective radius of 10  $\mu\text{m}$  and the effective variance of 0.1. The influence of varying particle size distributions is not studied in this work as Fischer and Grassl [29] showed the impact of the water droplet size is minor to the reflectance in oxygen A bands. The scattering matrix of water cloud is calculated with the Lorenz-Mie theory [30]. The lowest layer again consists of molecules only. The

vertical extent of the middle layer is determined by CTH and CGT. The lower boundary is an ocean surface with the surface roughness characterized by the Cox Munk model [31] with the wind speed. In this work the wind speed of 6 m/s is used for sensitivity study. CTH is measured from the ocean surface, which is always larger or equal to CGT. When CGT is equal to CTH, the bottom layer don't exist and the atmosphere becomes a two-layer system. The vertical profiles of the molecule number densities are determined by the 1976 US standard atmosphere [32].

## 3. Cloud masking over glint

Fig. 1(a) shows  $R_{764}/R_{780}$  of a clear sky case (COD = 0) for a typical Earth viewing geometry from EPIC, which reveals a near circular symmetrical pattern. The center circular region affected by the glint has low values of  $R_{764}/R_{780}$ , which is due to the strong glint radiance from the reference band of 780 nm. The ratio rises up when the viewing angle moves out of the glint and the atmosphere path length is relatively stable. Around the outer ring of the Earth the ratio decreases again because the reflectance in the reference band increases significantly due to enlarged scattering path length. Due to the near circular symmetry a line of pixels across the Earth image center is enough to represent the variability over the globe. Fig. 1(b) shows the ratio  $R_{764}/R_{780}$  for several values of COD over a horizontal line across the center of Fig. 1(a). Each pixel on the line has different solar incident and viewing angles, which are used in the radiative transfer simulator to calculate the reflectance ratios. It shows that  $R_{764}/R_{780}$  decreases as COD increases outside the glint affected area. The reason is that for the cases given here, the reflectance  $R_{780}$  increases more than  $R_{764}$  as the optical depth increases due to the oxygen absorption. Inside the glint area, the impact of COD on the ratio is reversed, i.e.,  $R_{764}/R_{780}$  increases if COD is larger, because  $R_{780}$  decreases as clouds block the intensity of sun glint. Fig. 1(c) shows that  $R_{780}$  outside of the glint area increases as COD increases, which is consistent with Fig. 1(b). At the center of the glint region,  $R_{780}$  decreases as COD increases when COD is relatively small (around 1). For a large value of COD (around 2),  $R_{780}$  will increase as COD increases as the glint is largely blocked out by clouds. Fig. 1(b) and 1(c) show that the ratio  $R_{764}/R_{780}$  varies with COD more sensitive than  $R_{780}$ . Furthermore, we can define the spatial gradient as the slope of  $R_{764}/R_{780}$  or  $R_{780}$  as a function of pixel index. The spatial gradient of  $R_{764}/R_{780}$  in Fig. 1(b) for a clear sky case is the largest compare with cases with nonzero COD, which can be used to increase the confidence level of cloud masking product near the edge of the sun glint disk for EPIC images.

## 4. Cloud height retrieval from the UV band

EPIC measurements in the oxygen A and B bands are sensitive to CTH and CGT. As we have reviewed in the introduction, the oxygen A and B band measurements are highly correlated so that only one parameter in CTH and CGT can be obtained after considering the impacts of noise [4]. To evaluate whether the UV bands can be used to determine CTH, Fig. 2 show the spectral reflectance of EPIC images for two viewing geometries:  $\theta_s = 20^\circ$ ,  $\theta_v = 20^\circ$ ,  $\phi_v = 170^\circ$ ; and  $\theta_s = 30^\circ$ ,  $\theta_v = 30^\circ$ ,  $\phi_v = 180^\circ$ , where  $\theta_s$ ,  $\theta_v$ , and  $\phi_v$  are the solar zenith angle (SZA), viewing zenith angle (VZA), and viewing azimuth angle relative to the solar principal plane (RAA), respectively. As expected, the oxygen A and B bands have the largest sensitivity on CTH. The reflectance at 388 nm increases as CTH increase in Fig. 2(b). The dependence however is not obvious for a different viewing geometry in Fig. 2(a). To show the overall picture, Fig. 3(a) shows the percentage difference of the reflectance at 388 nm between CTH = 5 km and CTH = 2.5 km. CGT is 2 km, and COD is 5.05 which is large enough so that the impact of sun

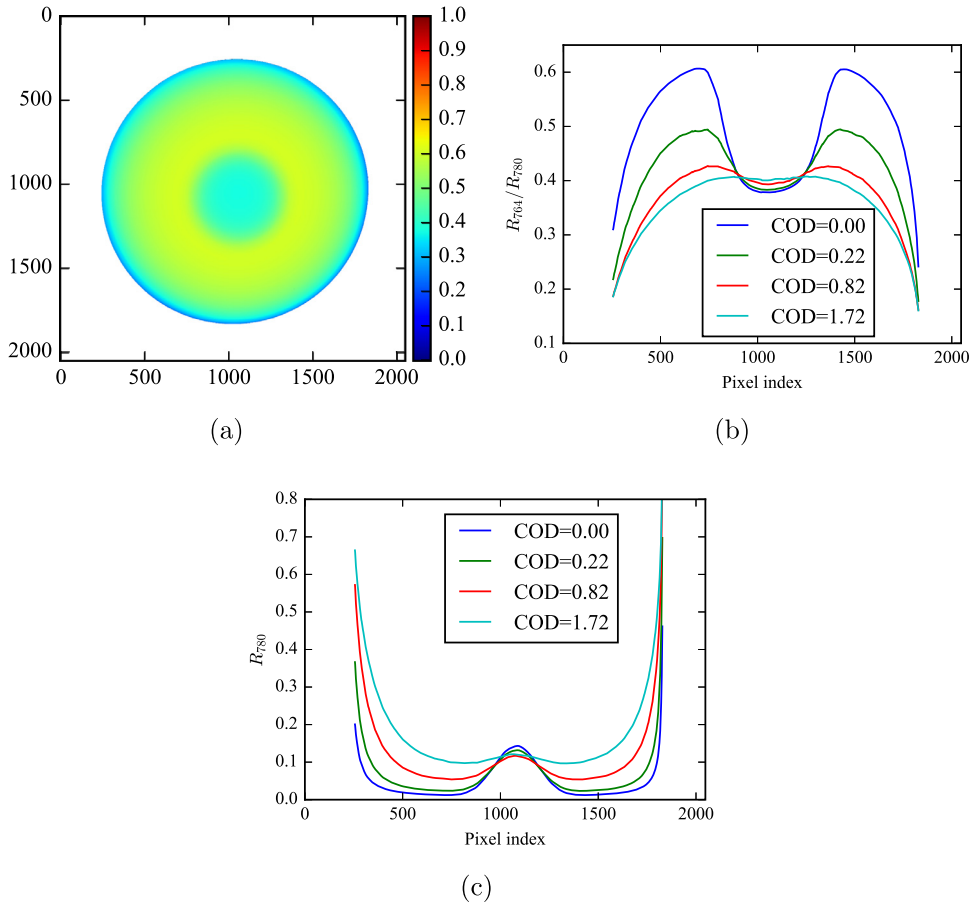


**Fig. 1.** (a)  $R_{764}/R_{780}$  of a clear sky case (COD is 0.0) for a typical Earth viewing geometry from EPIC. (b)  $R_{764}/R_{780}$  as a function of the pixel index on the horizontal line which intercept the image at  $y=1024$ , where  $y$  is the vertical pixel index. CTH and CGT are 2.5 and 1 km, respectively. (c)  $R_{780}$  on the same horizontal line as in Fig. 1(b).

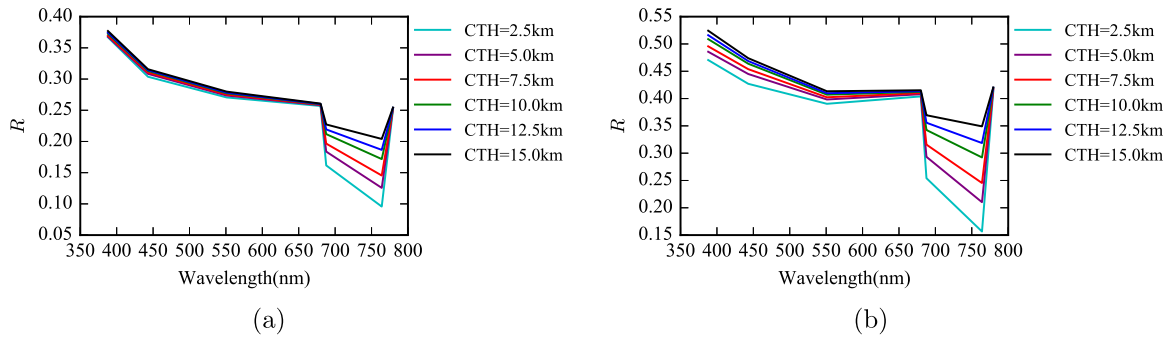


**Fig. 2.** The reflectance as a function of wavelength for two different viewing geometries. CGT and COD are 2 km and 5.05, respectively. (a) The solar zenith angle (SZA) is  $20^\circ$ , which is the same as the viewing zenith angle (VZA). The relative azimuth angle (RAA) is  $170^\circ$ . (b) SZA is  $30^\circ$ , which is the same as VZA. RAA is  $180^\circ$ .

glint is negligible. The absolute percentage difference between CTH = 5 km and CTH = 2.5 km is smallest at the center of the Earth's disk and becomes larger towards the rim of the Earth image. Geogdzhayev and Marshak [33] showed that the calibration of EPIC images is around 3% when normalized by the green band. If we assume 3% accuracy in the EPIC radiometric calibration, the CTH change of 2.5 km is only detectable at 388 nm for a ring area outside the center red and yellow region. Fig. 3(b) is the percentage difference between CTH = 10 km and CTH 2.5 km, which shows similar angular pattern as Fig. 3(a) but with larger magnitude. Around  $1/3 \sim 1/2$  of the center region the relative difference is still smaller than 3%. In summary it is difficult to use the 388 nm band to determine CTH at the center of EPIC images. However, the 388 nm band is helpful to find CTH for the outer ring region

with uncertainty of 2 - 3 km, if we assume 3% as the calibration uncertainty.

To investigate the impact of the possible CTH information from the 388 nm band to the CGT retrieval, Fig. 4 shows the ratio  $R_{abs}/R_{ref}$  as a function of CTH for a set of different CGT values, where the subscripts *abs* and *ref* stand for the oxygen A/B bands and their corresponding reference continuum bands, respectively. The cloud optical depth is 5.05 and both SZA and VZA are  $40^\circ$  and RAA is  $170^\circ$ . The oxygen B band ratio shows smaller displacement between consecutive CGT values than that of the oxygen A band. If CTH is known, the ratio  $R_{abs}/R_{ref}$  can be used to search the look-up-table represented by Fig. 4 to find CGT. For example, if  $R_{764}/R_{780} = 0.5$  and CTH = 8 km, Fig. 4 shows that CGT is less than but close to 6 km. A uncertainty in CTH would lead to uncertainty in CGT

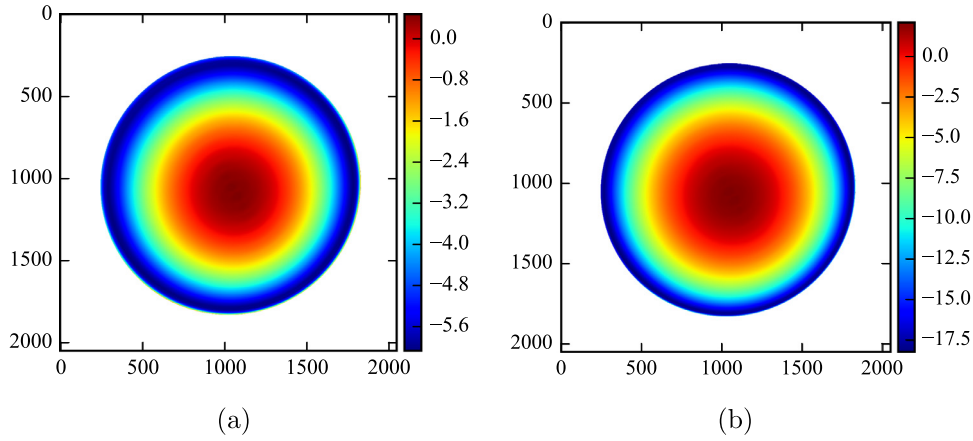


**Fig. 3.** (a) The percentage difference of the reflectance at 388 nm between CTH = 5 km and 2.5 km for a typical Earth viewing geometry from EPIC. COD is 5.05 and CGT is 2 km. (b) the same as Fig. 3(a) but for the difference between CTH=10 km and 2.5 km. Note the different colorbar scales in (a) and (b).

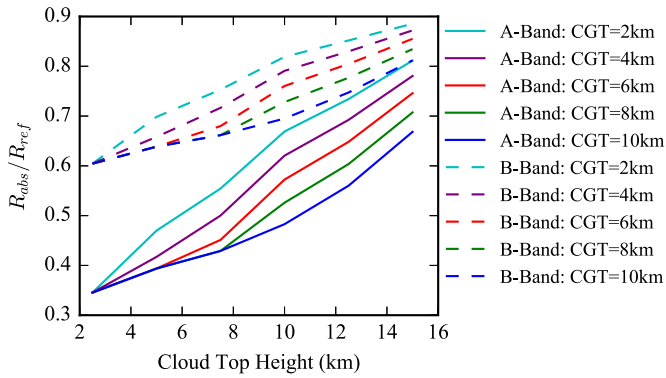


**Fig. 4.**  $R_{obs}/R_{ref}$  as a function of CTH for both the oxygen A and B bands. A set of different CGT are used. Cloud optical depth is 5.05, and SZA is  $40^\circ$ , which is the same as VZA. RAA is  $170^\circ$ .

determination. If  $R_{764}/R_{780} = 0.5$  and CTH = 10 km, an estimate of CGT would be close to 10 km from Fig. 4, so an uncertainty of 2 km in CTH would lead to an error of roughly 4 km for CGT. This estimate however depends on different  $R_{764}/R_{780}$  and CTH values as the look-up-table is not uniformly gridded.

## 5. Summary

In this paper we present a radiative transfer simulator for the DSCOVR/EPIC images. The radiative transfer model is based on the successive order of scattering method. Gas absorption due to ozone, oxygen, water vapor, nitrogen dioxide, methane, and carbon dioxide are included. The simulator is used to study the sensitivity of the EPIC bands to cloud parameters, including cloud masking, cloud optical depth, cloud top height, and cloud geometric thickness. The atmospheric reflectance increases as COD increases if the viewing angle is outside the sun glint region. Inside the sun glint region, the reflectance in non-absorbing bands does not have monotonic variation depending on the COD values. However, the ratio of the oxygen A/B bands to their continuum reference increases monotonically with respect to COD inside a circular region affected by the sun glint. The ratios  $R_{abs}/R_{ref}$  for the clear sky case has the largest spatial gradient which could be used to increase the cloud masking confidence level around the edge of the sun glint disk. In addition to the oxygen A and B bands, we studied the sensitivity of the reflectance at UV (388 nm) band to the CTH variation. We found that the 388 nm band has limited sensitivity in the center region of the Earth image to CTH. On the other hand,

the 388 nm band is sensitive to CTH for the ring region whose inner radius is larger than half of the Earth radius. If 3% accuracy is assumed for the calibration of the 388 band, the change of 2–3 km in CTH could be detected by this band for the outer ring region. This in turn leads to an uncertainty of 4 km in CGT retrieval based on the oxygen A and B bands look-up-table.

## Acknowledgments

This research was funded by NASA DSCOVR Earth Science Algorithms Program and NASA Grants (80NSSC18K0345 and NNX15AK87G).

## References

- [1] Marshak A, Herman J, Adam S, Karin B, Carn S, Cede A, et al. Earth observations from DSCOVR EPIC instrument. *Bull Am Meteorol Soc* 2018;99(9):1829–50. doi:10.1175/BAMS-D-17-0223.1.
- [2] Herman J, Huang L, McPeters R, Ziemke J, Cede A, Blank K. Synoptic ozone, cloud reflectivity, and erythemal irradiance from sunrise to sunset for the whole Earth as viewed by the DSCOVR spacecraft from the Earth–Sun lagrange 1 orbit. *Atmos Meas Tech* 2018;11(1):177–94. doi:10.5194/amt-11-177-2018.
- [3] Yang Y, Marshak A, Mao J, Lyapustin A, Herman J. A method of retrieving cloud top height and cloud geometrical thickness with oxygen A and B bands for the deep space climate observatory (DSCOVR) mission: radiative transfer simulations. *J Quant Spectrosc Radiat Transf* 2013;122:141–9. doi:10.1016/j.jqsrt.2012.09.017.
- [4] Davis AB, Ferlay N, Libois Q, Marshak A, Yang Y, Min Q. Cloud information content in EPIC/DSCOVR's oxygen A- and B-band channels: a physics-based approach. *J Quant Spectrosc Radiat Transf* 2018;220:84–96. doi:10.1016/j.jqsrt.2018.09.006.
- [5] Davis AB, Merlin G, Cornet C, Labonnote LC, Rédi J, Ferlay N, et al. Cloud information content in EPIC/DSCOVR's oxygen A- and B-band channels: an optimal estimation approach. *J Quant Spectrosc Radiat Transfer* 2018;216:6–16. doi:10.1016/j.jqsrt.2018.05.007.
- [6] Yang Y, Meyer K, Wind G, Zhou Y, Marshak A, Platnick S, et al. Cloud products from the earth polychromatic imaging camera (EPIC): algorithms and initial evaluation. *Atmos Meas Tech Discuss* 2018;2018:1–23. doi:10.5194/amt-2018-316.
- [7] Marshak A, Knyazikhin Y. The spectral invariant approximation within canopy radiative transfer to support the use of the EPIC/DSCOVR oxygen b-band for monitoring vegetation. *J Quant Spectrosc Radiat Transf* 2017;191:7–12. doi:10.1016/j.jqsrt.2017.01.015.
- [8] Lyapustin AI, Wang Y, Laszlo I, Hilker T, GHall F, Sellers PJ, et al. Multi-angle implementation of atmospheric correction for MODIS (MAIAC): 3. atmospheric correction. *Remote Sens Environ* 2012;127:385–93. doi:10.1016/j.rse.2012.09.002.
- [9] Martins JV, Tanré D, Remer L, Kaufman Y, Mattoo S, Levy R. MODIS Cloud screening for remote sensing of aerosols over oceans using spatial variability. *Geophys Res Lett* 2002;29(12):MOD4-1–MOD4-4. doi:10.1029/2001GL013252.
- [10] Banks AC, Mélin F. An assessment of cloud masking schemes for satellite ocean colour data of marine optical extremes. *Int J Remote Sens* 2015;36(3):797–821. doi:10.1080/01431161.2014.1001085.
- [11] Girolamo LD, Davies R. A band-differenced angular signature technique for cirrus cloud detection. *IEEE Trans Geosci Remote Sens* 1994;32(4):890–6. doi:10.1109/36.298017.



- [12] Ackerman SA, Strabala KI, Menzel WP, Frey RA, Moeller CC, Gumley LE. Discriminating clear sky from clouds with MODIS. *J Geophys Res* 1998;103(D24):32141–57. doi:[10.1029/1998JD200032](https://doi.org/10.1029/1998JD200032).
- [13] Frey RA, Ackerman SA, Liu Y, Strabala KI, Zhang H, Key JR, et al. Cloud detection with MODIS. part i: improvements in the MODIS cloud mask for collection 5. *J Atmos Oceanic Technol* 2008;25(7):1057–72. doi:[10.1175/2008JTECHA1052.1](https://doi.org/10.1175/2008JTECHA1052.1).
- [14] Marchand R. Trends in ISCCP, MISR, and MODIS cloud-top-height and optical-depth histograms. *J Geophys Res* 2013;118(4):1941–9. doi:[10.1002/jgrd.50207](https://doi.org/10.1002/jgrd.50207).
- [15] Mekler Y, Podolak M. Estimation of cloud top heights from satellite imagery. *Appl Opt* 1985;24(15):2419–22. doi:[10.1364/AO.24.002419](https://doi.org/10.1364/AO.24.002419).
- [16] Zhai P-W, Hu Y, Trepte CR, Lucker PL. A vector radiative transfer model for coupled atmosphere and ocean systems based on successive order of scattering method. *Opt Express* 2009;17(4):2057–79. doi:[10.1364/OE.17.002057](https://doi.org/10.1364/OE.17.002057).
- [17] Zhai P-W, Hu Y, Chowdhary J, Trepte CR, Lucker PL, Josset DB. A vector radiative transfer model for coupled atmosphere and ocean systems with a rough interface. *J Quant Spectrosc Radiat Transf* 2010;111(7):1025–40. doi:[10.1016/j.jqsrt.2009.12.005](https://doi.org/10.1016/j.jqsrt.2009.12.005).
- [18] Zhai P-W, Hu Y, Winker DM, Franz BA, Werdell J, Boss E. Vector radiative transfer model for coupled atmosphere and ocean systems including inelastic sources in ocean waters. *Opt Express* 2017;25(8):A223–39. doi:[10.1364/OE.25.00A223](https://doi.org/10.1364/OE.25.00A223).
- [19] Zhai P-W, Boss E, Franz B, Werdell PJ, Hu Y. Radiative transfer modeling of phytoplankton fluorescence quenching processes. *Remote Sens* 2018;10(8). doi:[10.3390/rs10081309](https://doi.org/10.3390/rs10081309).
- [20] Lenoble J, Herman M, Deuz J, Lafrance B, Santer R, Tanr D. A successive order of scattering code for solving the vector equation of transfer in the earth's atmosphere with aerosols. *J Quant Spectrosc Radiat Transf* 2007;107(3):479–507. doi:[10.1016/j.jqsrt.2007.03.010](https://doi.org/10.1016/j.jqsrt.2007.03.010).
- [21] Chowdhary J, Cairns B, Travis LD. Contribution of water-leaving radiances to multiangle, multispectral polarimetric observations over the open ocean: bio-optical model results for case 1 waters. *Appl Opt* 2006;45(22):5542–67. doi:[10.1364/AO.45.005542](https://doi.org/10.1364/AO.45.005542).
- [22] Zhai P-W, Kattawar GW, Yang P. Impulse response solution to the three-dimensional vector radiative transfer equation in atmosphere-ocean systems. i. Monte Carlo method. *Appl Opt* 2008;47(8):1037–47. doi:[10.1364/AO.47.001037](https://doi.org/10.1364/AO.47.001037).
- [23] Xu F, Davis AB, West RA, Martonchik JV, Diner DJ. Markov chain formalism for vector radiative transfer in a plane-parallel atmosphere overlying a polarizing surface. *Opt Lett* 2011;36(11):2083–5. doi:[10.1364/OL.36.002083](https://doi.org/10.1364/OL.36.002083).
- [24] Buehler SA, Eriksson P, Lemke O. Absorption lookup tables in the radiative transfer model ARTS. *J Quant Spectrosc Radiat Transf* 2011;112(10):1559–67. doi:[10.1016/j.jqsrt.2011.03.008](https://doi.org/10.1016/j.jqsrt.2011.03.008).
- [25] Rothman L, Gordon I, Babikov Y, Barbe A, Benner DC, Bernath P, et al. The hitran2012 molecular spectroscopic database. *J Quant Spectrosc Radiat Transf* 2013;130:4–50. doi:[10.1016/j.jqsrt.2013.07.002](https://doi.org/10.1016/j.jqsrt.2013.07.002). HITRAN2012 special issue.
- [26] Daumont D, Brion J, Charbonnier J, Malicet J. Ozone UV spectroscopy i: absorption cross-sections at room temperature. *J Atmos Chem* 1992;15(2):145–55. doi:[10.1007/BF00053756](https://doi.org/10.1007/BF00053756).
- [27] Bogumil K, Orphal J, Homann T, Voigt S, Spietz P, Fleischmann O, et al. Measurements of molecular absorption spectra with the SCIAMACHY pre-flight model: instrument characterization and reference data for atmospheric remote-sensing in the 230–2380 nm region. *J Photochem Photobiol, A* 2003;157(2):167–84. doi:[10.1016/S1010-6030\(03\)00062-5](https://doi.org/10.1016/S1010-6030(03)00062-5). Atmospheric Photochemistry.
- [28] Hansen JE, Travis LD. Light scattering in planetary atmospheres. *Space Sci Rev* 1974;16(4):527–610. doi:[10.1007/BF00168069](https://doi.org/10.1007/BF00168069).
- [29] Fischer J, Grassl H. Detection of cloud-top height from backscattered radiances within the oxygen a band. part 1: theoretical study. *J Appl Meteorol* 1991;30(9):1245–59. doi:[10.1175/1520-0450\(1991\)030<1245:DOCTHF>2.0.CO;2](https://doi.org/10.1175/1520-0450(1991)030<1245:DOCTHF>2.0.CO;2).
- [30] Mishchenko MI, Travis LD, Lacis AA. *Scattering, absorption, and emission of light by small particles*. Cambridge, U.K.: Cambridge University Press; 2002.
- [31] Cox C, Munk W. Measurement of the roughness of the sea surface from photographs of the sun's glitter. *J Opt Soc Am* 1954;44(11):838–50. doi:[10.1364/JOSA.44.000838](https://doi.org/10.1364/JOSA.44.000838).
- [32] on Extension to the Standard Atmosphere USC. U.S. standard atmosphere, 1976. U.S. Government Printing Office, Washington, D.C.: National Oceanic and Atmospheric Administration; 1976.
- [33] Geogdzhayev IV, Marshak A. Calibration of the DSCOVR EPIC visible and NIR channels using MODIS terra and aqua data and EPIC lunar observations. *Atmos Meas Tech* 2018;11(1):359–68. doi:[10.5194/amt-11-359-2018](https://doi.org/10.5194/amt-11-359-2018). <https://www.atmos-meas-tech.net/11/359/2018/>